Journal of Simulation and Analysis of Novel Technologies in Mechanical Engineering
17 (4) (2025) 0019~0046
DOI 10.71939/jsme.2025.1220027

Research article

Design of a dual solar-electric indoor lighting reinforcement system

Mostafa Pirmoradian*, Mohammad Hashemian, Ali Mokhtarian

Department of Mechanical Engineering, Kho.C., Islamic Azad University, Khomeinishahr, Iran

*pirmoradian@iaukhsh.ac.ir

(Manuscript Received --- 03 Oct. 2025; Revised --- 23 Dec. 2025; Accepted --- 29 Dec. 2025)

Abstract

The increasing energy consumption in the country is becoming one of the major economic and social problems. Although our beloved country is very rich in fossil and non-renewable energy resources, inefficient energy consumption imposes irreparable damage on the country's budget and ultimately makes the future unclear. The high cost of electricity production on the one hand and the limited consumption on the other hand, in addition to the previous reasons, double the importance of improving consumption and using more renewable resources. In the present study, the design of a system has been investigated, which can be used to reduce electricity consumption to zero for daytime lighting and greatly reduce energy consumption for nighttime lighting. The aim of this study is to generally investigate the use of solar energy and lighting in reducing electrical energy consumption. It is clearly visible that the high cost of solar equipment has limited the attention of consumers and energy engineers to using this type of production. Therefore, in this work, much attention has been paid to the simplicity and cheapness of the design and an attempt has been made to produce this system with the minimum equipment available in the Iranian market. In order to ensure the accuracy of the results obtained, the results were first compared with other valid results, which showed acceptable accuracy in all sections. The results obtained show that in the sunlight receiving section, which is the main focus of this research, the final designed trackers achieve high accuracy. By using instantaneous tracking in this system, we always benefited from this accuracy in practice. The next sections of the system are presented as an analytical design and a suitable combined system for lighting and providing light to buildings is introduced. According to the results obtained, the initial claim of the efficiency of this system and reducing electricity consumption has been proven.

Keywords: Lighting system, Solar tracker, Lighting amplifier, Solar-electric dual system.

1- Introduction

The global transition toward renewable energy has intensified research into maximizing the efficiency of photovoltaic (PV) systems, with solar tracking technologies emerging as a pivotal solution for enhancing energy yield. Fixed PV panels, while simple and cost-effective, suffer from suboptimal energy capture due to the sun’s changing position throughout the day and year, leading to significant efficiency losses [1-4]. Active solar trackers, which dynamically adjust the orientation of PV modules to maintain perpendicular alignment with solar rays, have been shown to substantially increase energy output—often by 20–40% compared to static systems [1-9].

Solar tracking systems are generally categorized into single-axis and dual-axis designs. Single-axis trackers follow the sun's daily east-west movement, offering a balance between performance improvement and system simplicity [1, 3, 9]. Dual-axis trackers, however, adjust both azimuth and elevation, enabling optimal alignment throughout the year and across diverse geographic locations, and are particularly effective in regions with high solar variability [4-14]. Recent reviews highlight dual-axis solar photovoltaic tracking (DASPT) as a fundamental technology for maximizing solar energy capture, with energy yield improvements up to 85–90% under optimal conditions [12].

The performance of active trackers depends heavily on their control algorithms and sensor technologies. Early systems relied on light-dependent resistors (LDRs) to detect sunlight intensity, but these are limited by saturation and low-visibility conditions [1-5]. Innovations such as ultraviolet (UV) sensors [5], GPS-based orientation [11, 15, 16], and adaptive neuro-fuzzy inference systems (ANFIS) [17] have improved tracking accuracy, robustness, and adaptability. Hybrid control strategies, combining open-loop sun position algorithms with real-time feedback, further enhance performance under variable weather [7]. The integration of artificial intelligence and machine learning is a promising trend for optimizing control and reducing operational costs [12, 17].

While active trackers entail higher initial investment and maintenance costs than fixed or single-axis systems, their long-term benefits include increased energy production, favorable payback periods, and adaptability to mobile or high-altitude applications [8, 11, 12, 15, 16]. Economic analyses confirm that dual-axis trackers are especially advantageous in areas with high solar resource variability [8, 12]. Additionally, the use of advanced materials and recycling strategies can further improve the sustainability of PV systems [9].

Despite significant progress, challenges remain in optimizing tracker reliability, reducing costs, and adapting to diverse environmental conditions. Future research is expected to focus on advanced control algorithms, integration with smart grids, and the development of lightweight, robust mechanical designs for broader deployment [12, 16-18].

In summary, active solar tracking systems represent a mature and rapidly evolving field, offering substantial gains in PV system efficiency and supporting the global shift toward sustainable energy solutions [5-12].

Among the various solar tracking strategies reported in the literature, including GPS-based positioning, open-loop sun path algorithms, and artificial intelligence–assisted controllers, electro-optical tracking systems offer a favorable compromise between tracking accuracy, system complexity, and implementation cost. GPS-based and purely algorithmic approaches rely heavily on precise calibration, geographical data, and uninterrupted computational performance, which may limit their reliability under variable environmental conditions or increase system cost. In contrast, electro-optical tracking provides real-time feedback based on actual solar irradiance, enabling continuous self-correction in the presence of transient cloud cover, atmospheric scattering, or installation misalignments. These characteristics make electro-optical trackers particularly suitable for low-cost and locally manufacturable systems, where simplicity, robustness, and adaptability are critical design constraints. Accordingly, an electro-optical tracking strategy was selected in this study to ensure reliable real-time solar alignment while maintaining economic feasibility and compatibility with the available components in the Iranian market.

In this study, a dual solar-electric lighting system enhanced by an electro-optical active solar tracker is designed and evaluated. The novelty lies on the integrated design of a dual solar-electric indoor lighting system that simultaneously combines electro-optical solar tracking, photovoltaic power generation, and direct daylight transmission through optical fibers. Unlike many existing studies that focus

solely on PV efficiency improvement, this work emphasizes a low-cost, locally manufacturable solution tailored to Iranian market constraints, while also addressing indoor lighting reinforcement and visual comfort.

2- Modeling, design, and formulation of the active solar tracking

This research project is composed of two main subsystems: the solar-optical system and the photovoltaic (PV) system. Both require high tracking accuracy to maximize efficiency, and after evaluating various tracking options, an electro-optical tracking system was selected for its balance of precision and cost-effectiveness. Three control circuits were designed and analyzed, with the optimal one chosen for implementation. The complementary subsystems were analytically evaluated due to market limitations in Iran (see Section 3 in [PDF]).

2-1- Structural design principles

Environmental factors such as wind, temperature fluctuations, precipitation, and wildlife significantly affect the durability and performance of solar tracking systems. Therefore, the system structure was designed to ensure robustness against these elements, maintaining stable operation even under adverse conditions. Initial scale models were built to identify potential structural weaknesses before constructing the main frame.

The primary structure uses steel with modular gear sets designed for smooth and accurate motion transmission (see Fig. 1).

Rack-and-pinion arrangements allow rotation of the movable structure around a fixed base. The gear setup provides coverage of solar azimuth movement from 0 to 240 degrees, sufficient to cover the sun's trajectory in Iranian cities such as Shiraz and Isfahan.

Fig. 1 The built structure with tracking equipment and solar panels

Linear motors (jacks) with a stroke of 30 cm and a gear diameter of approximately 18 cm were selected to provide the required rotation angle with high precision and torque.

Two linear electric motors were chosen for their smooth operation, low speed, high durability, and energy efficiency. Their design allows stable movement even under strong winds, supported by a robust steel base capable of carrying the entire tracking assembly.

2-2- Electro-optical tracking principles

The electro-optical tracker relies on detecting light intensity differences between paired photoresistors (LDRs). These LDRs are arranged in a specific configuration, where differential resistance changes correspond to the sun's incident angle variations.

2-2-1 Components and working method of the basic tracking system

2-2-1-1 Electronic Circuit

This basic system, which represents the first designed circuit, is founded on the balanced resistance between two photoresistors (light-dependent resistors) arranged appropriately (Figure 2).

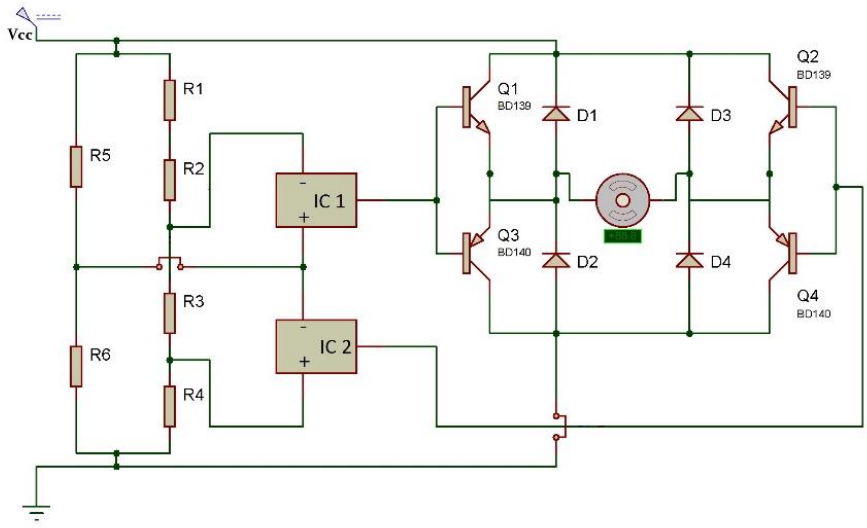

Fig. 2 Basic electrical circuit based on the working of amplifier and transistor

This circuit, serving as the foundational circuit for many tracking systems, required testing under the geographic conditions of Iran to evaluate its advantages and disadvantages for practical utilization. Considering two amplifiers with equal gain (IC1, IC2), the circuit output (the potential difference across the motor terminals) is calculated by the following equation:

$$V_M = \frac{R_6 \times (2R_1 + 2R_2 + R_3) - R_5 \times (R_3 + 2R_4)}{(R_1 + R_2 + R_3 + R_4) \times (R_5 + R_6)} \times V_{CC} \quad (1)$$

which R_5 and R_6 are the resistances resulting from the two light-dependent resistors (LDRs). The motor stress ratio is equal to zero. Its relationship is shown in the following equation:

$$\frac{R_6}{R_5} = \frac{R_3 + 2R_4}{2R_1 + 2R_2 + R_3} \quad (2)$$

In this circuit, the resistance values were selected according to experimental tests as: $R_1 = 50K\Omega,\ R_2 = 15K\Omega, R_3 = 10K\Omega,$ $and\ R_4 = 47K\Omega$

The applied resistance values used have an ohmic ratio $\frac{R_6}{R_5}$ equal to 0.75 or $\frac{1}{0.75}$. This means that for a specific value of this ratio between R_1 and R_2, the output is set to zero. When this ratio increases beyond this range, the motor rotates clockwise, and when it falls below this range, it rotates counterclockwise. Therefore, this value determines the sensor accuracy.

2-2-1-2- System theory

LDRs have a very high resistance (in this work $2M\Omega$), which decreases upon receiving light and direct irradiation. In this case, the specific resistance values for light reception (inactive state of the LDR in the presence of sunlight) and direct irradiation (active state of the LDR in the presence of sunlight) are 419Ω and 205Ω, respectively. These values may vary if a light filter is used.

Table 1: Specific resistance of LDRs in different conditions

	In direct sunlight	In the diffusion of sunlight
Specific resistance of LDRs with conventional filter	288Ω	1.5$k\,\Omega$
Specific resistance of LDRs with complete filter	550Ω	2.5$k\,\Omega$

The specific resistance of the LDR can be expressed as follows:

$$R = R_1 - \Delta R_{Incident} = R_1 - KI_{max}\cos\alpha \quad (3)$$

where I_{max} is the direct solar irradiance and α is the solar radiation emission angle. Figure 3 shows the pyramidal arrangement of two sensors

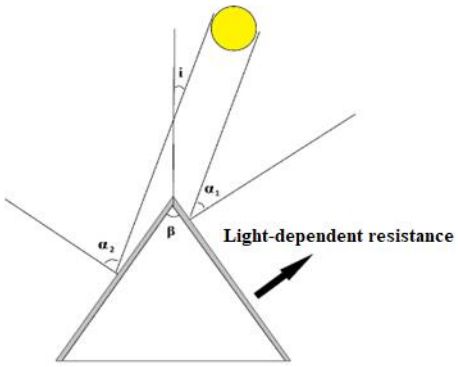

Fig. 3 Sensor layout and sun radiation angles

The angles used were obtained from Eqs. 5 and 6.

$$\alpha_1 = \frac{\pi - \beta}{2} - i \quad (5)$$

$$\alpha_2 = \frac{\pi - \beta}{2} + i \quad (6)$$

Using Eqs. 5 and 6, the Ohmic ratio will be as follows:

$$\Omega = \frac{R_1 - KI_{max}\cos\alpha_2}{R_1 - KI_{max}\cos\alpha_1} = \frac{R_1 - KI_{max}\cos[\frac{\pi-\beta}{2} + i]}{R_1 - KI_{max}\cos[\frac{\pi-\beta}{2} - i]} \quad (7)$$

The curve of this equation is provided in Fig. 4.

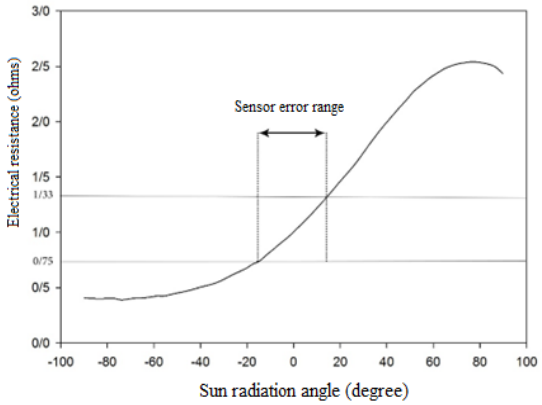

Fig. 4 Numerical curve of Ohmic change

The relative values of the emission angles were set for the values of 0.75 and 1.33 the ohmic ratio $\Omega = \frac{R_6}{R_5}$. The differences between the angles corresponding to this event represent the system errors. The driving force for the movement of the two axes is provided by two DC linear motors of 12_{volt}. The system configuration is horizontal, and the sensor orientation towards the sun is achieved by motor rotation. Various pyramidal sensors (at angles of 30°, 60°, 90°, 120°, and 135°) were examined to study the effect of the beta angle on system accuracy. For each studied angular position, the specific resistance of each LDR was measured using a digital multimeter. The specific resistance values used for each angle of this event were taken from the curve of the solar radiation angle and the optical resistance shown in Fig. 5. This chart represents the steady-state value of the specific resistance when the inactive face of the LDR is oriented

towards the sun. However, this trend decreases following a cosine relationship when the active face faces the sun. This decrease aligns well with the equation proposed in the theoretical framework of the research. The ohmic ratio of the specific resistance $(\Omega = 0.75, 1.33)$ for the studied pyramidal sensors is illustrated in Figure 6. The intersection of these two curves reveals the angular accuracy of the sensor.

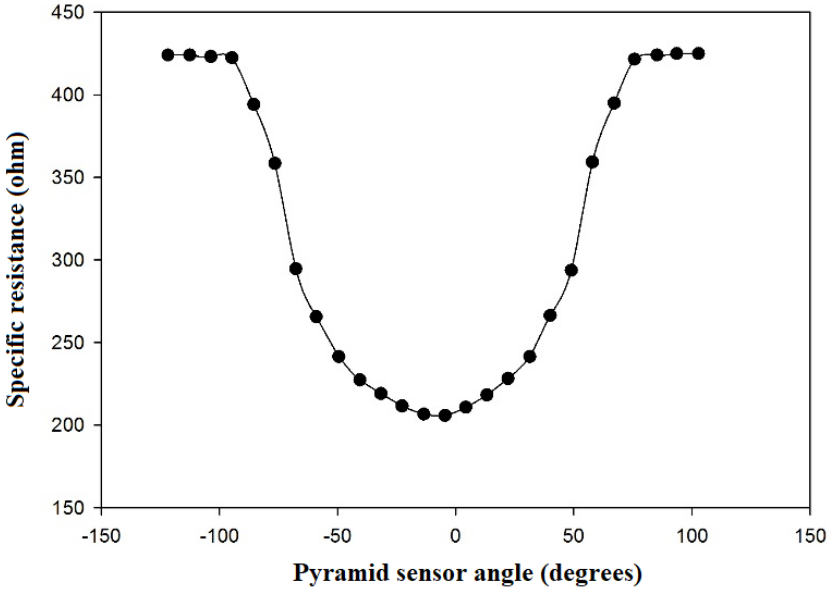

Fig. 5 LDR characteristic curve

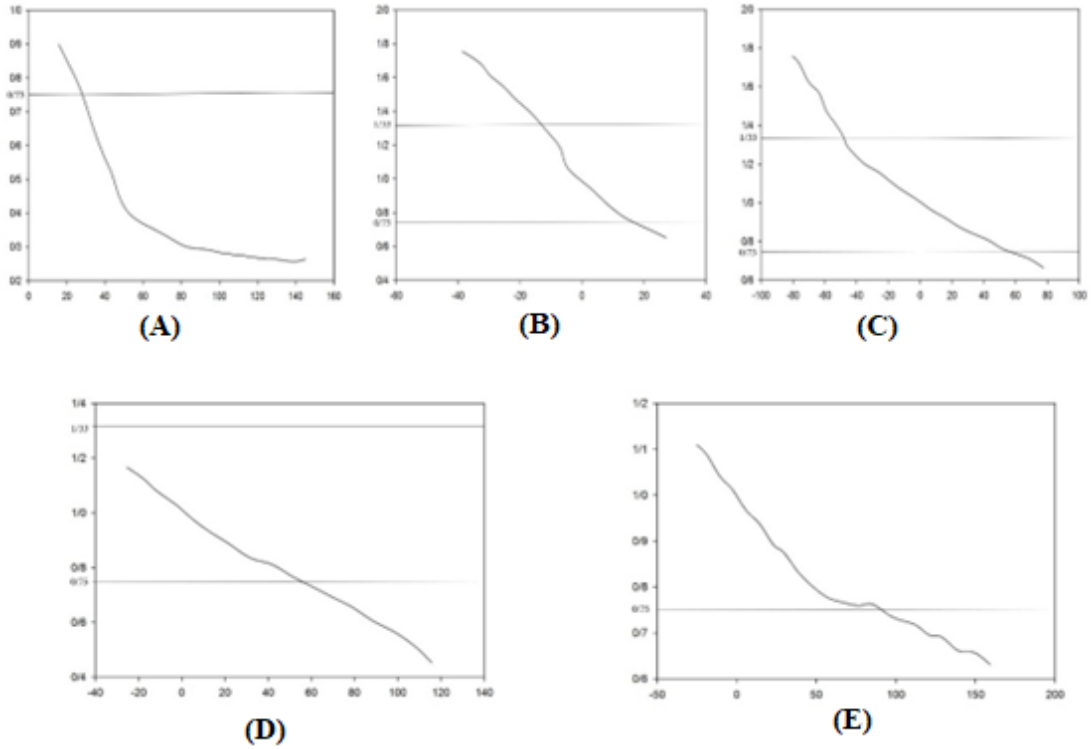

Fig. 6 Rate of change of LDR resistance for different angles of sunlight for different angles of the sensor

pyramid

Although according to references, the 60-degree angle was introduced as the optimal angle for the triangular sensor configuration, experiments were conducted on other angles to evaluate the minimum error at different angles. The results of these experiments confirmed the superiority of the 60-degree angle compared to other angles.

Fig. 7 Prototype of pyramid-shaped sensor structure built

3- Components and working method of the developed tracking system

Practical implementation of electro-optical solar tracking systems is often challenged by signal noise, motor jitter, and control instabilities arising from the analog nature of light-dependent resistor (LDR) sensors and nonlinear electronic components. In the initial prototype developed in this study, such effects manifested as intermittent oscillations and abrupt azimuthal movements, particularly under fluctuating irradiance conditions. To systematically address these limitations, the tracking system was refined through a multi-stage development approach. In the first stage, the control circuit was reconfigured by replacing transistor-based actuation with diode–relay logic to suppress unintended current leakage and reduce motor stress. In the second stage, buffer-based signal conditioning was introduced to convert analog sensor outputs into discrete binary states, effectively eliminating noise-induced ambiguity and ensuring stable, deterministic motor control. This staged development strategy enabled progressive improvement of tracking stability while preserving the simplicity and low-cost objectives of the system.

3-1- The first stage

In this stage, the same prior theory is used, and the sensor structure remains the aforementioned pyramidal form. In the previous system, multiple instabilities and jumps were observed in azimuth tracking. These jumps, caused by the control circuit structure, can subject the motor to ohmic stress and reduce its lifespan, in addition to being undesirable control behavior for tracking. Therefore, components must be employed in the circuit design to reduce these errors and maintain the system's stability as much as possible. Although transistors amplify the voltage for motor activation, their nonlinear behavior and leakage current in the inactive region contribute to such circuit behavior, causing occasional instabilities. Hence, transistors should be replaced by other elements where possible to improve these jumps.

Common-cathode diodes create specific electronic conditions that can be leveraged complementarily with electronic relays to enhance the system. By establishing a better control circuit for the motors, these jumps can be prevented. Among common-cathode diodes, the determining diode is the one activated at a higher voltage. When this diode activates, it passes the voltage applied to its anode to the shared cathode, preventing other diodes from activating and blocking current flow through their branches, while its branch remains active. This condition is utilized in this research. When one diode becomes active and determining, it turns on the electronic relay in its branch. According to the relay connections

to the motor, the motor's rotation direction is set, and the motor remains active until the two optical sensors receive equal light.

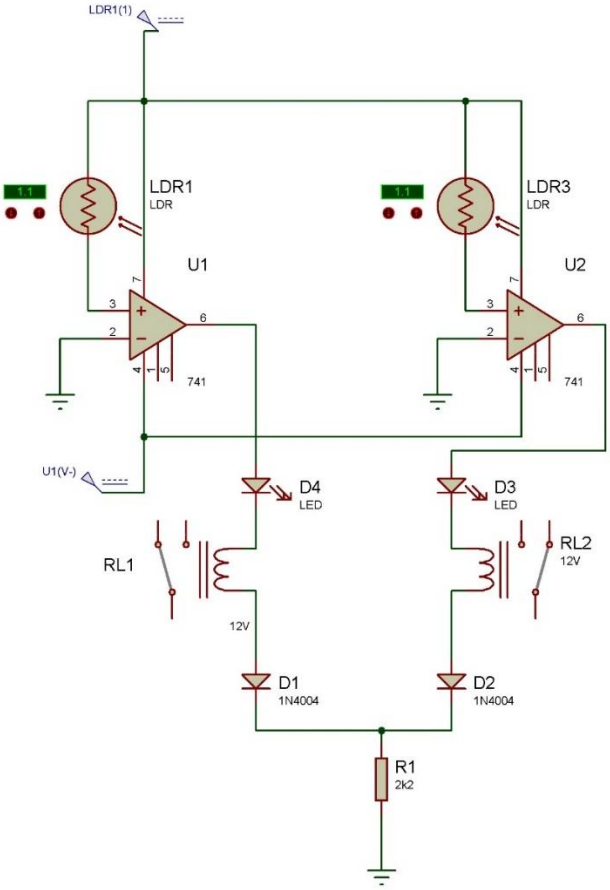

Fig. 8 The electrical circuit developed in the first stage is based on the work of the amplifier and diode.

In this stage, as shown in Figure 9, efforts have also been made to improve the sensor structure.

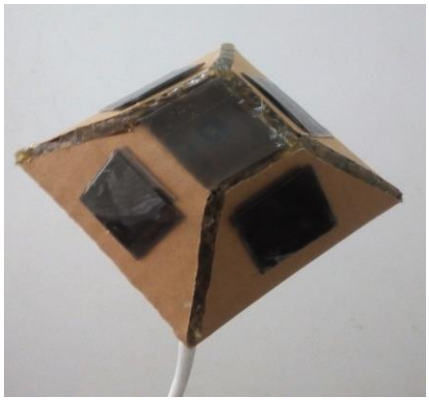

Fig. 9 Sensor structure developed in the first stage

3-2- The Second Stage

Although in the first stage of development, the use of new components eliminated the jumps of the base system and the system achieved desirable operational stability approaching the theoretical azimuth predictions, further alignment is required to ensure the system consistently faces the sun. Besides improving the efficiency of solar panels, the solar concentration system must achieve optical stability to provide stable illumination. Since this system performs light focusing, tracking must be instantaneous to maintain the stability of critical system points, such as keeping the focal point aligned with the optical fiber.

To stabilize tracking and enhance system accuracy, the best achievable electronic solution is to eliminate noise from the sensor data. The issues present in the base and secondary systems arise from analog control, which is inherently prone to noise and resolution limitations. In the second stage of

development, the goal is to evaluate sensor data digitally with noise-free conversion.

The practical and applied solution implemented in this stage uses buffers, specifically the ULN2003A model. The function of the buffer in this system is that any input voltage higher than its common base voltage grounds the corresponding output pin, setting its voltage to zero. The output pins of this buffer typically have the same voltage as their common base voltage. Consequently, the buffer outputs switch between two states:

- Absence of voltage (zero or less than half a volt)
- Presence of voltage (12 or 5 volts)

These states correspond to binary zero and one. This approach effectively eliminates noise and stabilizes the system. Therefore, relays connected to buffers always have two states: off or on. The "on" state occurs only when the voltage from the two-stage comparison of optical sensor signals activates the related buffer input pin.

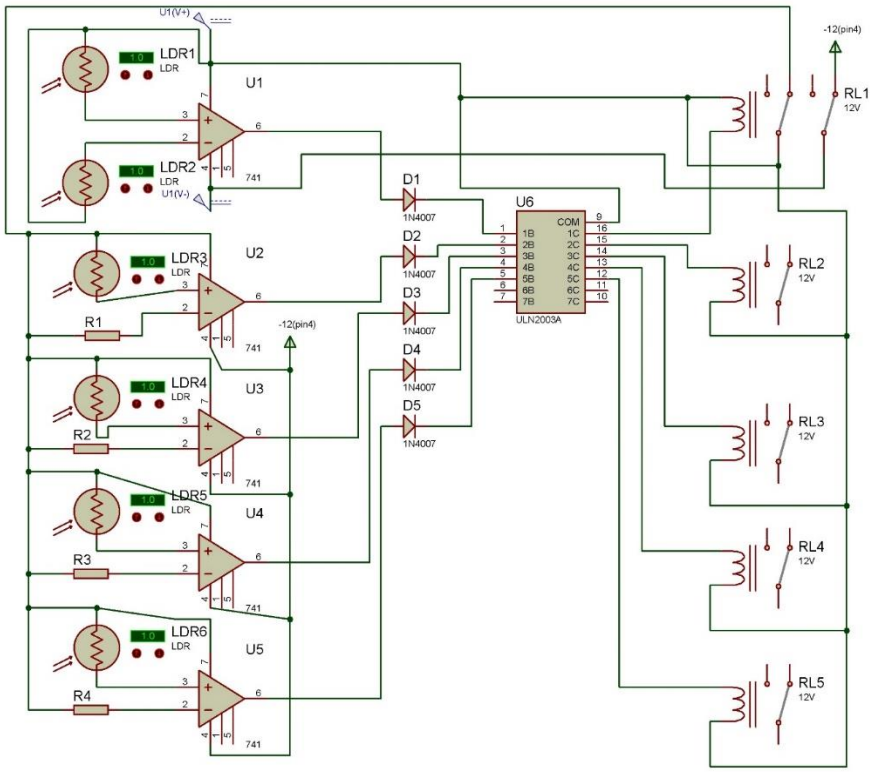

Fig. 10 The detector circuit developed in the second stage

Operational amplifiers (op-amps) in the system function as voltage comparators, similar to previous circuits. However, op-amp number one compares the voltages of two sensors responsible for restarting and initiating system activity in the morning. One sensor is installed on the panel and the other behind it so that if the light received behind the panel exceeds that on the panel under any conditions, the system stops activity and directs itself towards the region offering greater illumination. This is particularly relevant in early morning when the system may have halted at the last tracking stage from the previous day. This problem was previously identified by references, and this solution appears suitable to address it, especially since the tracker is also used for optical solar systems. It is preferable that the tracker always orients towards the brighter area.

Diodes permit only positive voltage to pass, so as long as the op-amps' outputs are not

positive, no activating voltage reaches the buffer. In other op-amps, voltage from the sensor is compared against a reference voltage set by a resistor for the comparison base. This implementation improves overall system responsiveness and accuracy in directing the solar tracking system.

The value of this resistance was determined experimentally $2.2k\Omega$ based on the test location and environmental conditions. Therefore, the sensor voltage becomes decisive when the sensor resistance is less than this value and supplies a higher voltage to the op-amp. According to the results of these comparisons, the buffer determines which relay to activate. Based on the relay circuit shown in the schematic, the activated relays specify how the motors should orient themselves.

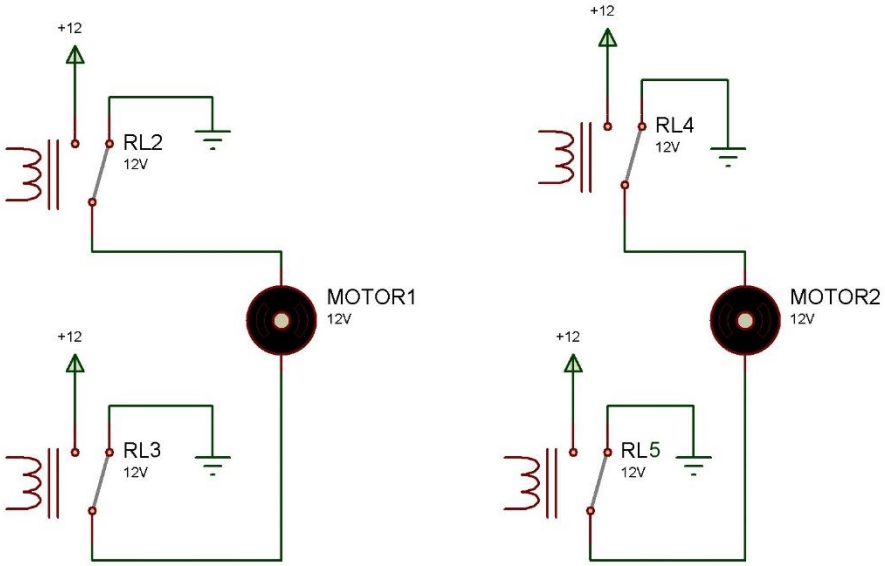

Fig. 11 Circuit connecting relays to motors

The activity of the motors can be described according to the relay function in Tables 2 and 3. In these tables, zero means the motor is off, one means the motor is on and rotating clockwise, and minus one indicates the motor is on and rotating counterclockwise. This representation clarifies how the relays control the motors' operation and orientation direction based on the system's electrical signals.

Table 2: How the M1 motor works according to the relays' activity

RL2	*RL3*	*M1*
0	0	0
0	1	-1
1	0	1
1	1	0

Table 3: How the M2 motor works according to the relays' activity

RL4	*RL5*	*M2*
0	0	0
0	1	-1
1	0	1
1	1	0

In this system setup, if motor M1 rotates counterclockwise and the linear jack is closed, the system moves from east to west. If motor M1 rotates clockwise and the linear jack opens, the system moves from west to east. Similarly, for motor M2, which controls the tracking system in the north-south direction, clockwise rotation and opening the linear jack moves the system north towards zenith, while counterclockwise rotation and closing the linear jack directs the system towards the horizon.

When both relays are on, the motor inputs are supplied with 12V, so there is no voltage difference across the motor inputs, and the motor remains off. Although by using relays that control multiple switches, special wiring can avoid this situation, ensuring no voltage output reaches the motor when both relays are active.

4- Control circuit and noise reduction

The initial circuit design showed instabilities including motor jitter and tracking oscillations in azimuth positioning due to analog control and transistor nonlinearities. To mitigate these, buffers (ULN2003A) and diode networks were added to stabilize outputs and prevent motor overdrive (Figures 12).

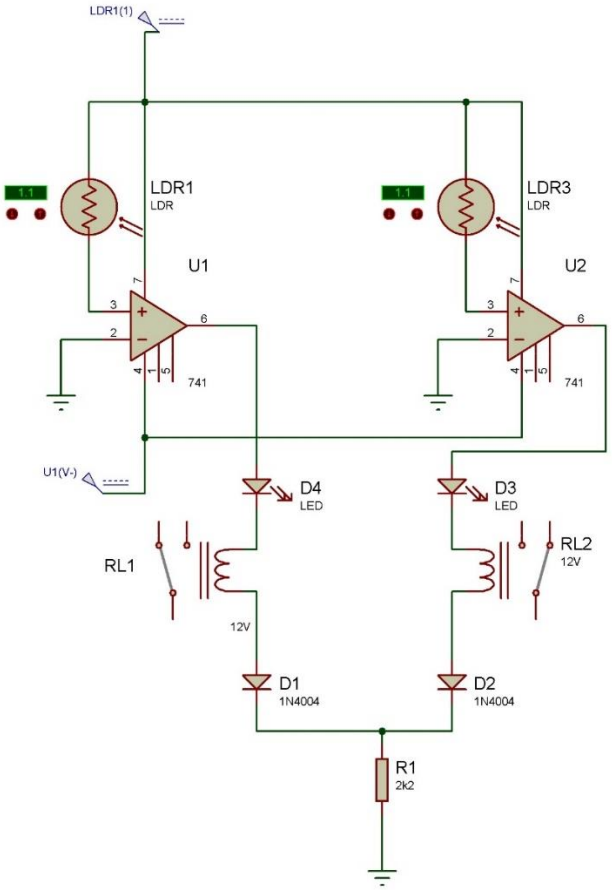

Fig. 12 The electrical circuit developed in the first stage based on the work of the amplifier and diode.

Relay circuits control motor direction with on/off states clearly defined. Two relays per motor manage clockwise and counterclockwise rotation (Tables 3-2 and 3-3).

Operational amplifiers (op-amps) are used to compare sensor voltages and initiate motor activation at dawn or after cloudy conditions when the system must reacquire the sun's position.

5- System integration

The photovoltaic subsystem uses a commercial 10 W solar panel (Figure 13), chosen to evaluate the benefits of the tracker. Power generated is fed into a converter to charge batteries and supply DC loads such as LED lighting. An inverter converts stored DC power to AC for general electrical loads when sunlight is insufficient. LEDs were selected for their low power consumption and compatibility (Figure 14).

Fig. 13 Specifications of the solar panel used

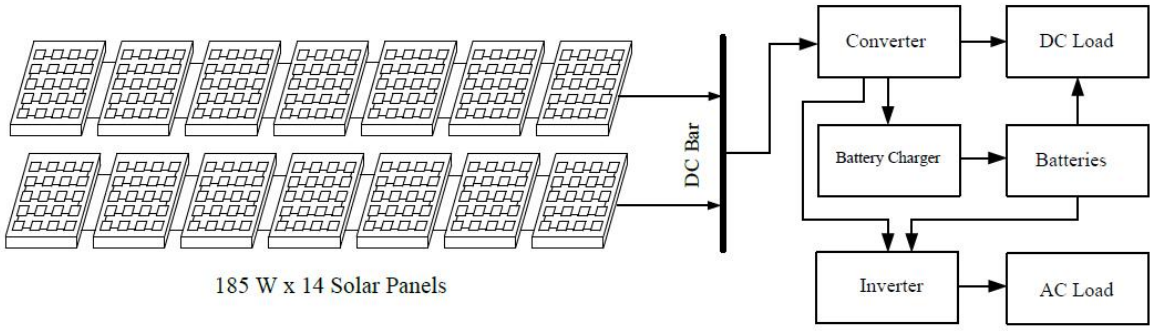

Fig. 14 Block diagram of the grid connected to the photovoltaic system

5-1- Optical concentration and light transmission

The solar-optical system collects sunlight via large convex lenses concentrating light onto optical fiber cables (Figure 15). These fibers transmit natural light indoors, reducing electric lighting needs during the day. Light concentration efficiency ranges from 20% to 30%, complementing the PV electricity generation for overall energy savings.

5-2- Lighting control and visual comfort

Indoor lighting is controlled by sensors assessing ambient light levels. The system balances artificial lighting activation to maintain light intensity within visual comfort zones (lux levels) appropriate for various environments—offices, industrial workplaces, sports facilities (Tables 4 and 5).

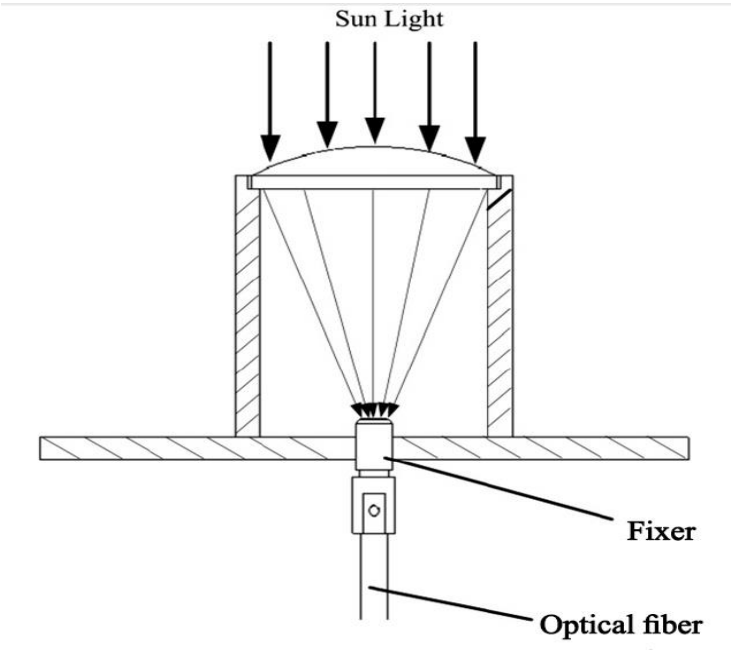

Fig. 15 The sunlight concentrator at the beginning of the optical fiber

Table 4: Required lighting intensity in different locations

Desired location	Illumination intensity (Lux)

Office, workplace	500
Passageways	100
Restaurant and cafe	200
Industrial warehouses	100
Design and mapping location	750
Classroom	300

Table 5: Lighting intensity required for different sports

Desired sport	Illumination intensity (Lux)
Football, basketball, volleyball, judo, hockey, etc.	300
Football, basketball, volleyball, etc. (in progress)	500
Badminton, tennis, ping-pong, fencing, etc.	500
Badminton, tennis, ping-pong, fencing, etc. (in progress)	750
Boxing	300
Boxing (in progress)	1500-3000

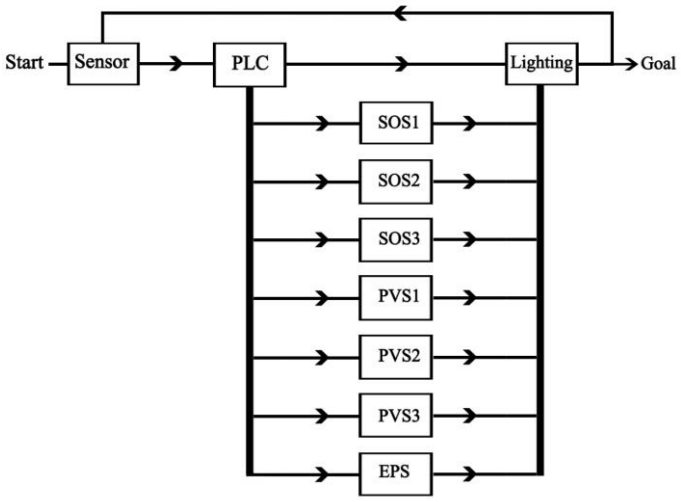

Fig. 16 Flowchart of the lighting process at the target location

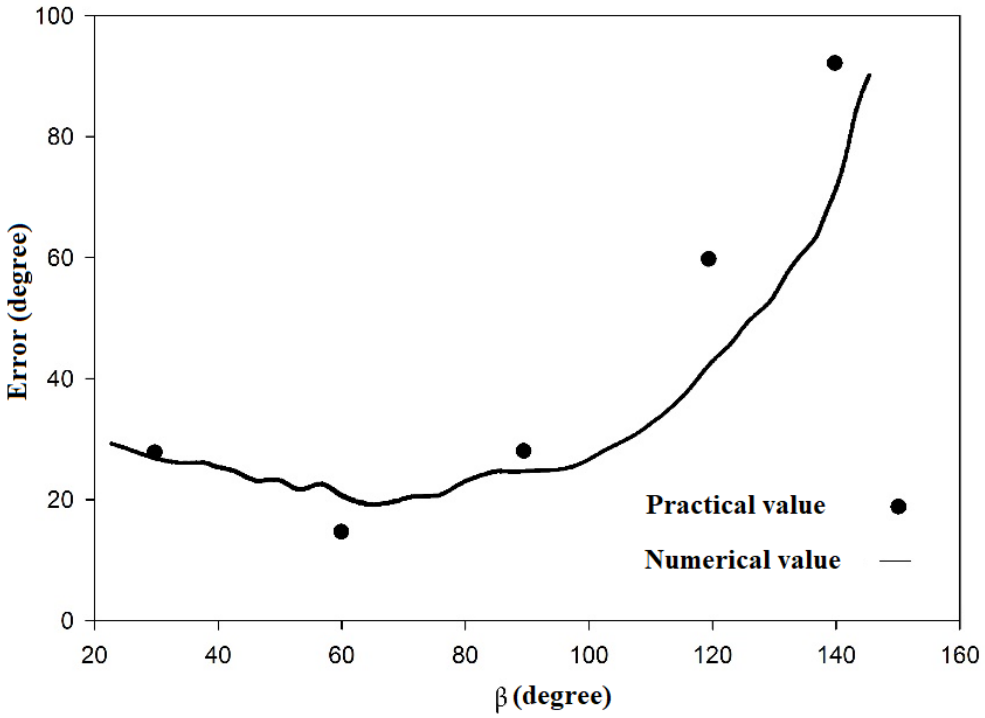

Fig. 17 Comparison of numerical errors in the reference with practical errors for different angles

6- Validation of the tracking system

In the previous chapter, we reviewed the overall system workflow and identified the roles of each subsystem. It is essential to evaluate the performance and correctness of these subsystems to ensure that the research follows proper principles and the experimental work aligns with similar studies. Therefore, this chapter compares the developed system with analogous systems from previous research and thoroughly examines the problem addressed by this study.

The sensor structure was manufactured in a pyramidal shape and evaluated at various angular positions. Different tracking errors were recorded and compared with numerical errors reported in the literature. Figure 17 illustrates this comparison, showing a good agreement between experimental and predicted errors under various environmental conditions.

A preliminary prototype of an electro-optical solar tracking circuit was tested under the climatic conditions of Shiraz, Iran. The results were benchmarked against previous studies to validate the research methodology and experimental setup.

Several comparative analyses have been conducted on energy production by fixed versus tracked photovoltaic (PV) panels in different locations worldwide. Figures 18 to 20 display comparative power outputs in Aswan (Egypt), Berlin (Germany), and Stuttgart (Germany) respectively [19].

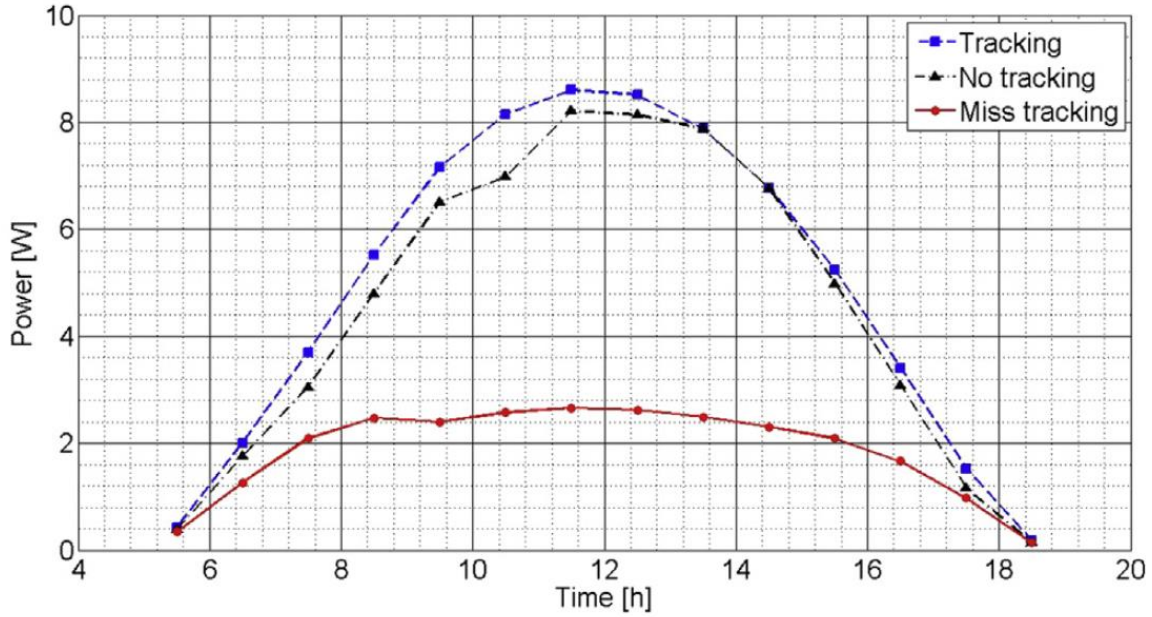

Fig. 18 A comparison between energy generated by fixed and tracked PV panels in the city of Aswan, Egypt [19].

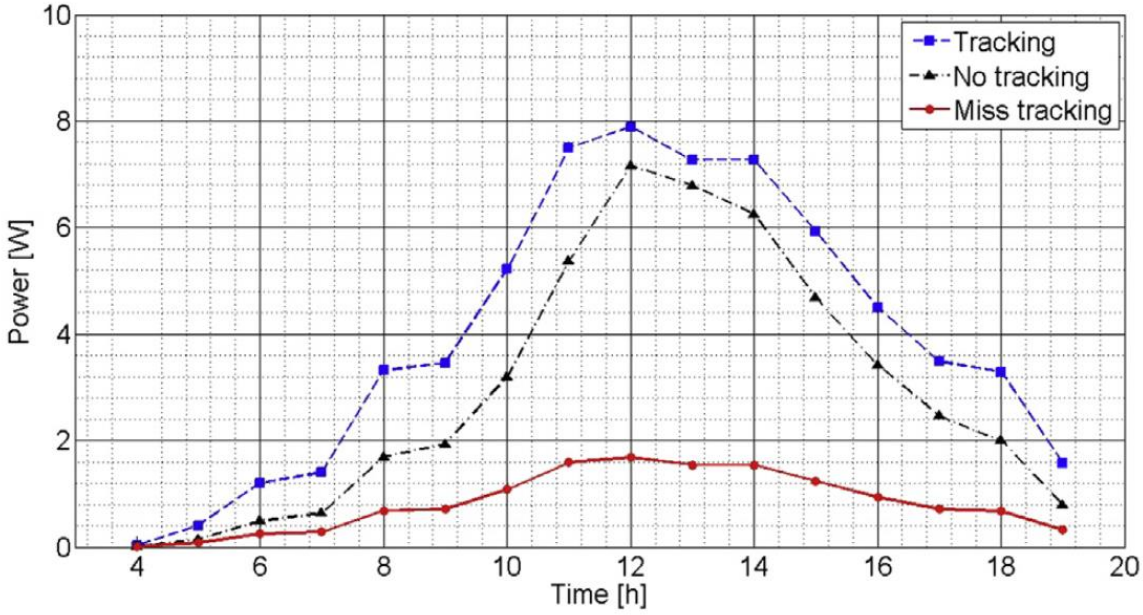

Fig. 19 A comparison between energy generated by fixed and tracked PV panels in Berlin, Germany [19].

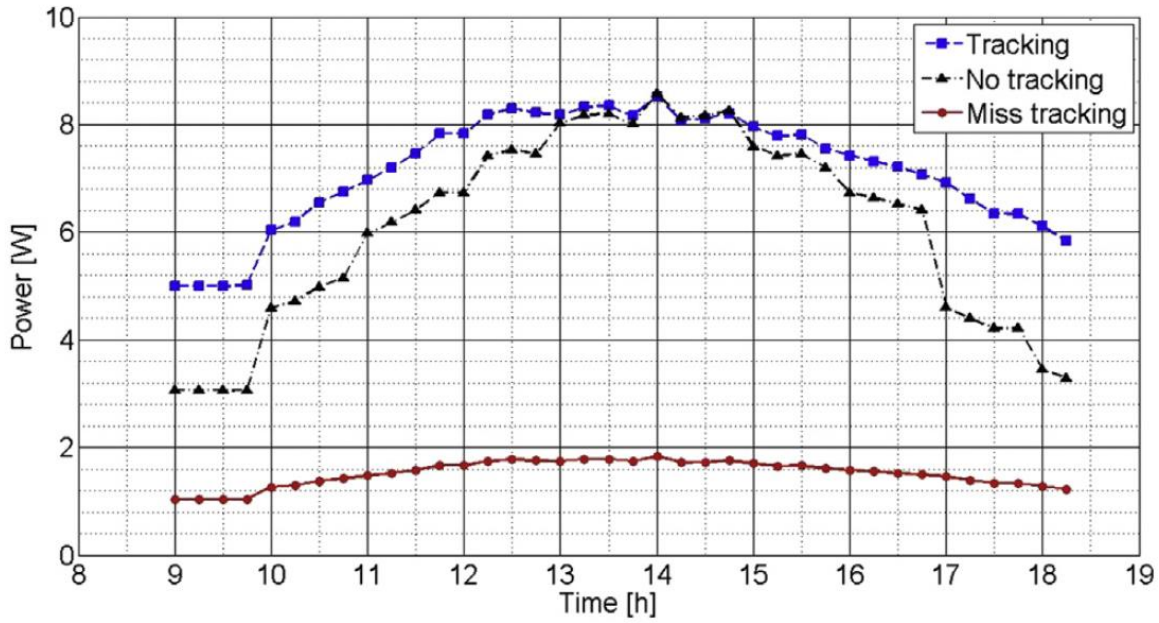

Fig. 20 A comparison between energy generated by fixed and tracked PV panels in Stuttgart, Germany [19].

These results demonstrate that solar tracking systems significantly increase PV panel efficiency. In the current study, the tracking sensor design closely resembles those in the referenced works, and similar efficiency improvements have been experimentally confirmed. Figure 21 compares power output of fixed and single-axis tracked PV panels with the original sensor and control circuit used here, showing appreciable efficiency gains consistent with global research trends.

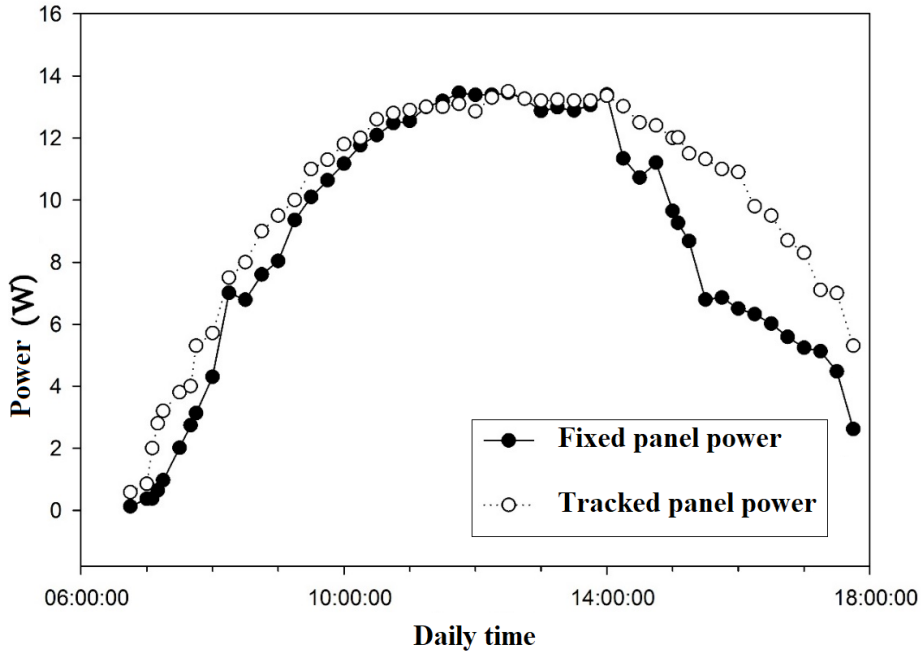

Fig. 21 A comparison between the energy generated by fixed and tracked PV panels in the east-west axis in the present study

It is noted that solar irradiance patterns and therefore tracking system performance vary among different geographic locations. Minor structural differences among tracking systems provide insights into design optimization tailored to specific conditions.

A key design objective in this work has been the capability for real-time solar azimuth and altitude tracking, as accurate, continuous orientation toward the sun maximizes energy capture.

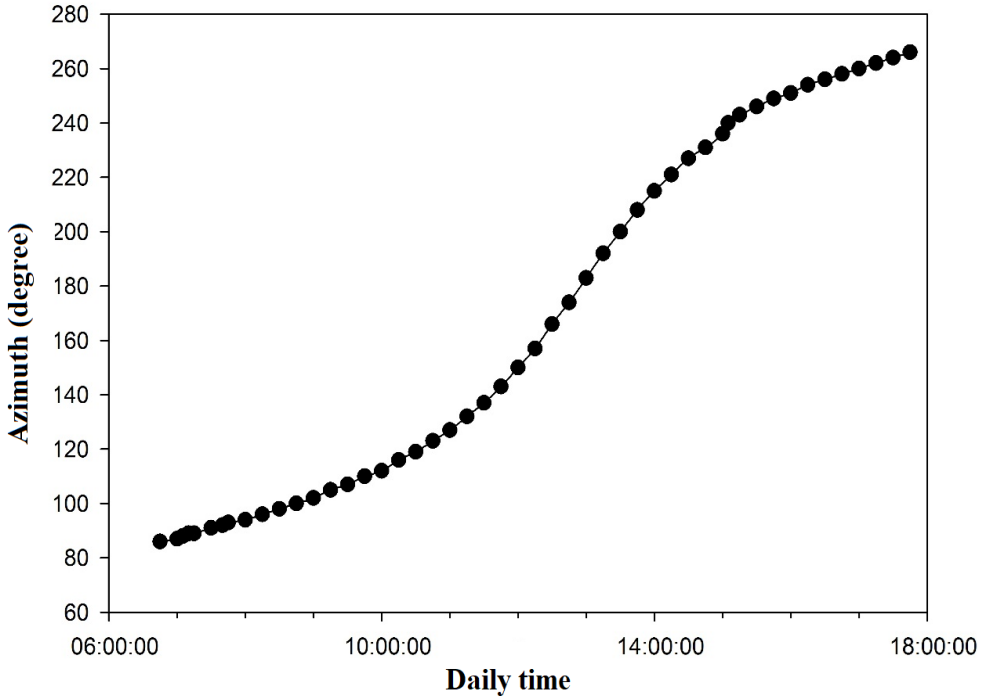

Fig. 22 Daily azimuth trend for the test site, extracted from the Australian Geosciences Complex.

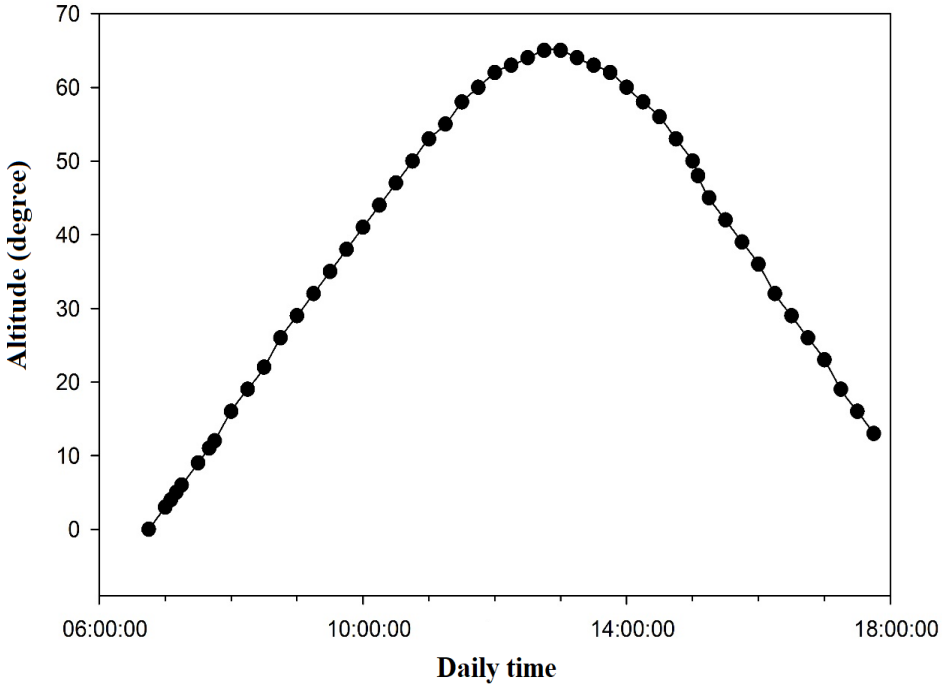

Fig. 23 Daily altitude trend for the test site, extracted from the Australian Geosciences Complex.

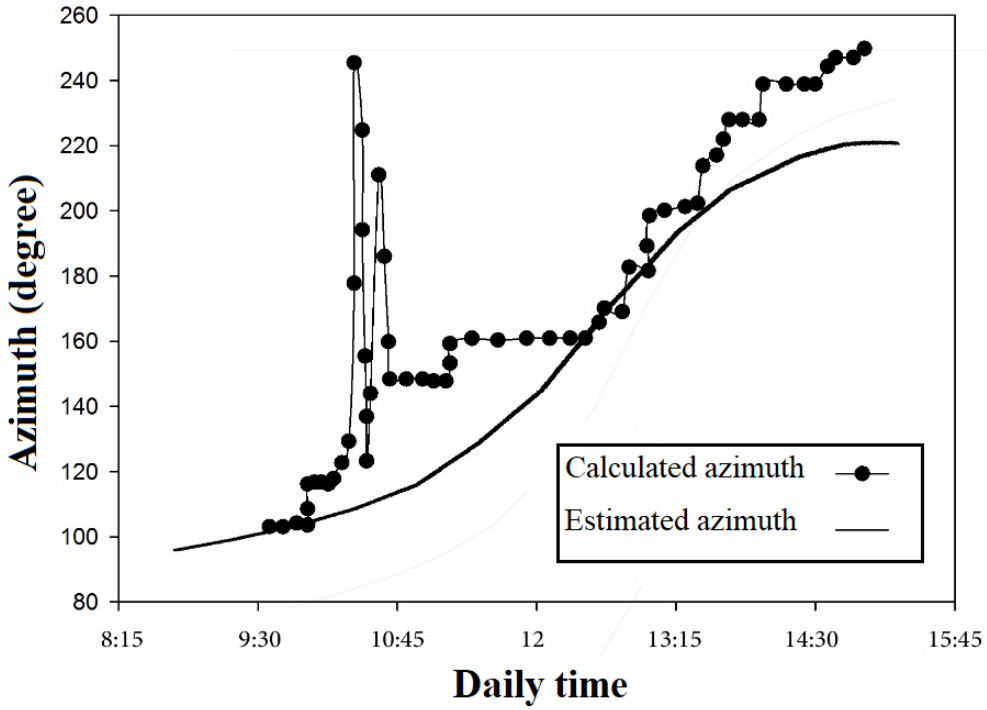

Fig. 24 The azimuth calculated practically in the initial tracking and the azimuth estimated from the mentioned references.

Daily azimuth and altitude changes for the test location are shown in Figures 22 and 23 respectively, extracted from Australian geographic data. These demonstrate solar elevation angles typically peaking near but not exceeding 65° during summer, an important consideration in system range design.

Figure 24 presents a comparison between estimated and actual tracked solar azimuth angles using the initial control circuit, further validating system accuracy against trusted geographic data.

7- Results analysis

The present study investigates the impact and effectiveness of three custom-designed solar tracking circuits. These circuits' performance is evaluated by measuring the improvement in photovoltaic output power, comparing the tracked system to static panels. Additionally, the system continuously monitors solar coordinates using the supplementary control circuit to optimize alignment.

7-1- Power output analysis

The performance of the proposed solar tracking system was evaluated by comparing the electrical power output of the photovoltaic panel under different tracking configurations. Figure 25 illustrates the power output of a fixed photovoltaic panel during daylight hours. As expected, the generated power gradually increases after sunrise, reaches a maximum of approximately 9.5 W near solar noon, and then decreases toward sunset. The relatively narrow high-power interval and the reduced output during morning and late afternoon hours highlight the limitations of fixed installations in maintaining optimal orientation with respect to the sun’s trajectory.

Figure 26 presents the power output obtained using the initial tracking circuit. Compared to the fixed panel, the tracked system exhibits a noticeable improvement in peak power, reaching approximately 12.5 W, and maintains higher output levels over an extended portion of the day.

However, minor fluctuations and irregularities are observed in the power curve, particularly during periods of changing irradiance, which can be attributed to sensor noise and control instabilities inherent to the primary analog circuit.

Further improvements are evident in Figure 27, which corresponds to the first-stage developed tracking circuit. In this configuration, the power output curve becomes smoother and more consistent throughout the day, with peak power increasing to around 14.3 W. The reduction in oscillations reflects enhanced sensor discrimination and improved motor actuation stability, allowing the panel to more closely follow the sun's path even under moderately variable lighting conditions.

The power output achieved using the final optimized tracking circuit is shown in Figure 28. This configuration delivers the highest peak power, approximately 15.5 W, and sustains elevated power generation over the longest daily interval. The curve exhibits minimal oscillations and demonstrates rapid stabilization following short-term irradiance variations, such as transient cloud cover or partial shading. This behavior indicates that the final control strategy effectively suppresses noise-induced disturbances and enables continuous real-time correction of panel orientation, preventing prolonged power losses during non-ideal environmental conditions.

A cumulative comparison of the fixed panel and the successive tracking configurations is presented in Figure 29. The results clearly demonstrate the progressive enhancement in daily energy harvest achieved through each stage of system development, with the final tracking system yielding nearly a 60% increase in total energy output relative to the fixed configuration. This improvement underscores the practical advantage of the developed tracker, particularly in real-world operating conditions where irradiance fluctuations are unavoidable.

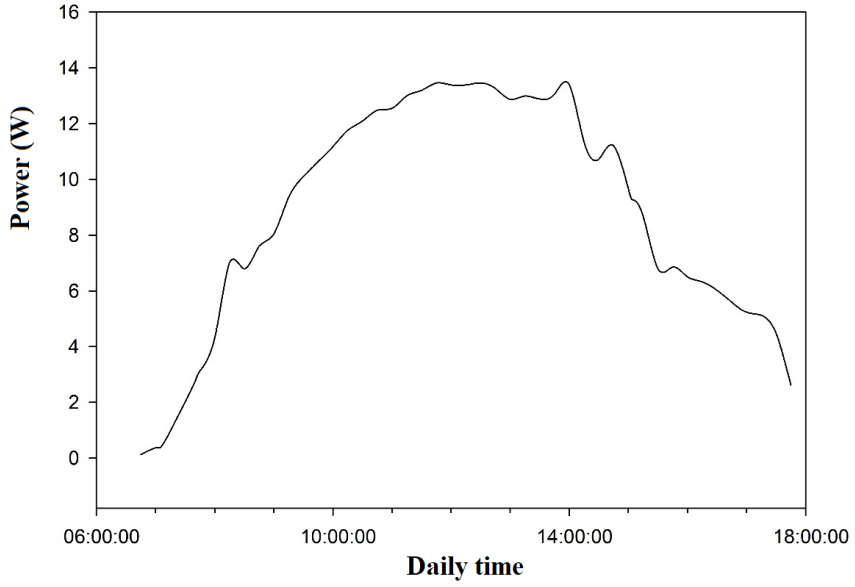

Fig. 25 Fixed panel output power during daytime hours

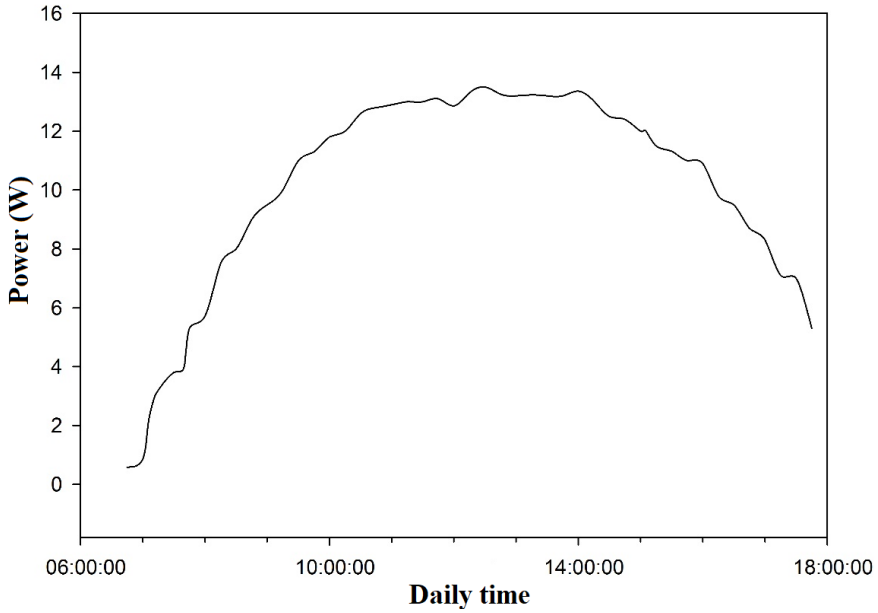

Fig. 26 Panel output power tracked with primary circuit during daytime hours

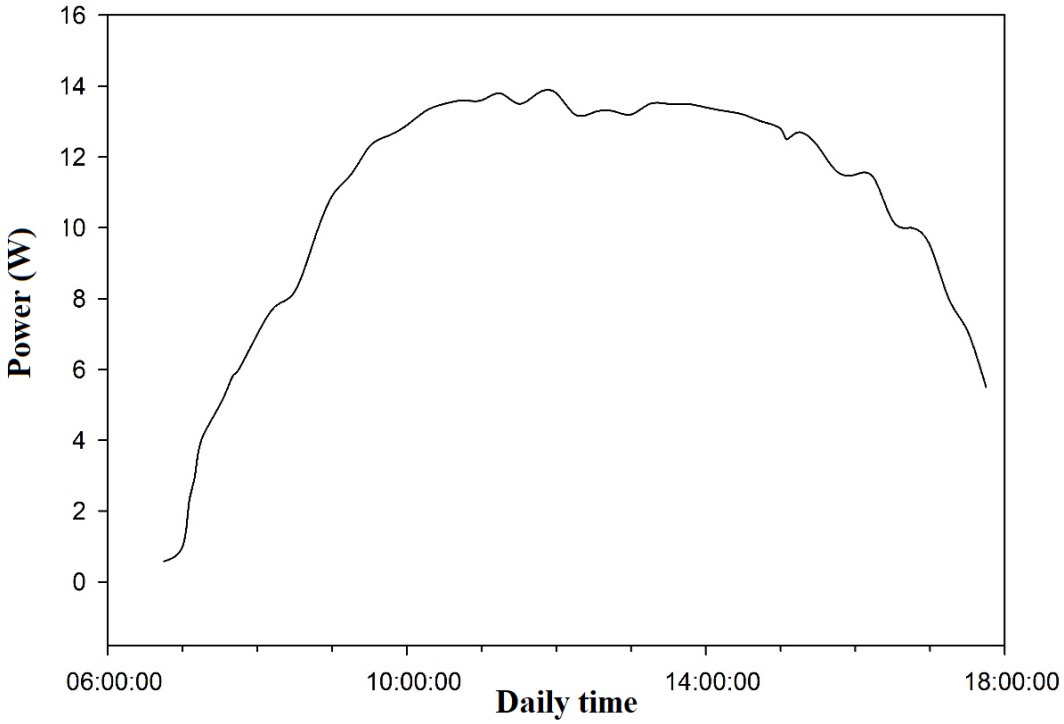

Fig. 27 Panel output power tracked with the developed circuit in the first stage during daylight hours

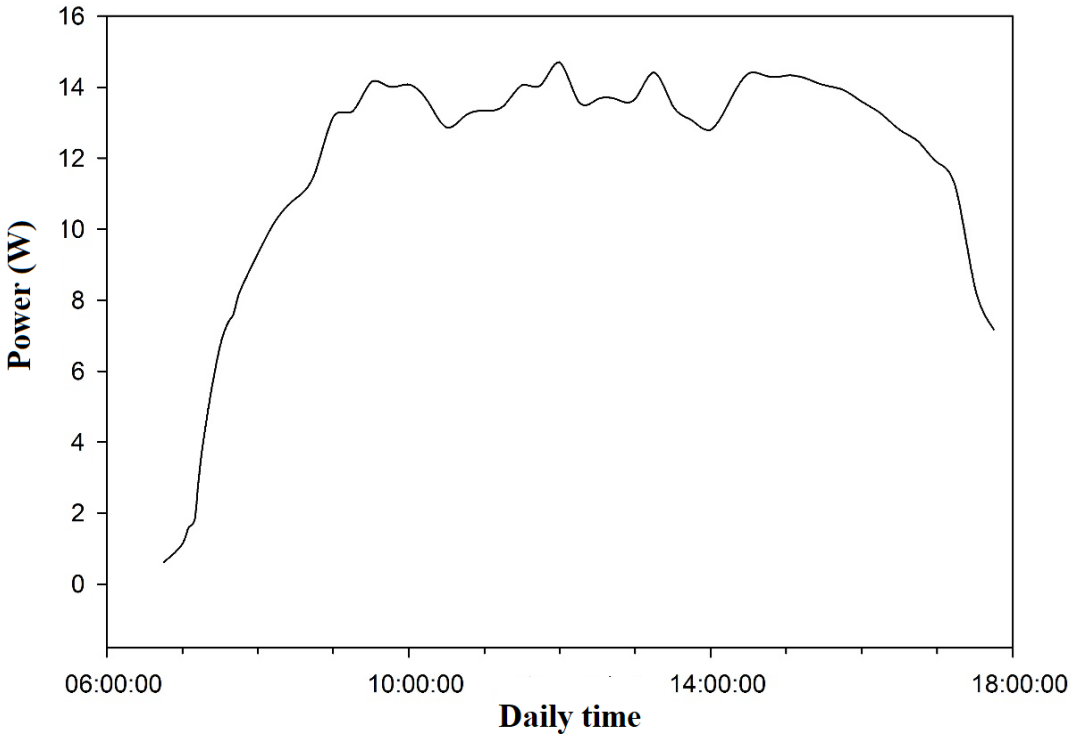

Fig. 28 Panel output power tracked with final circuit during daytime hours

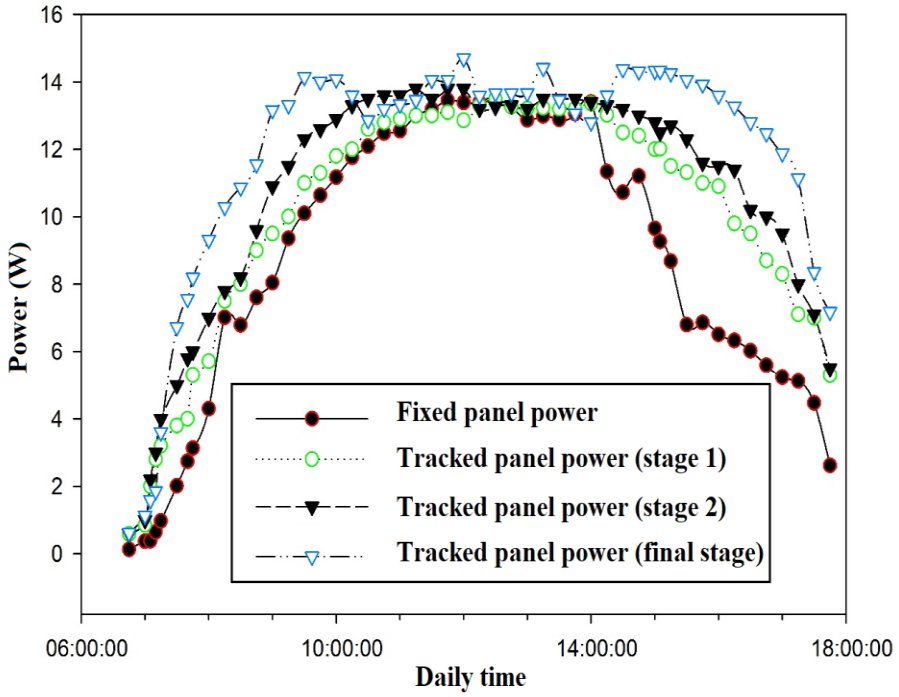

Fig. 29 Comparison between the output powers of the fixed panel, the tracked panel with the initial circuits and those developed in later stages

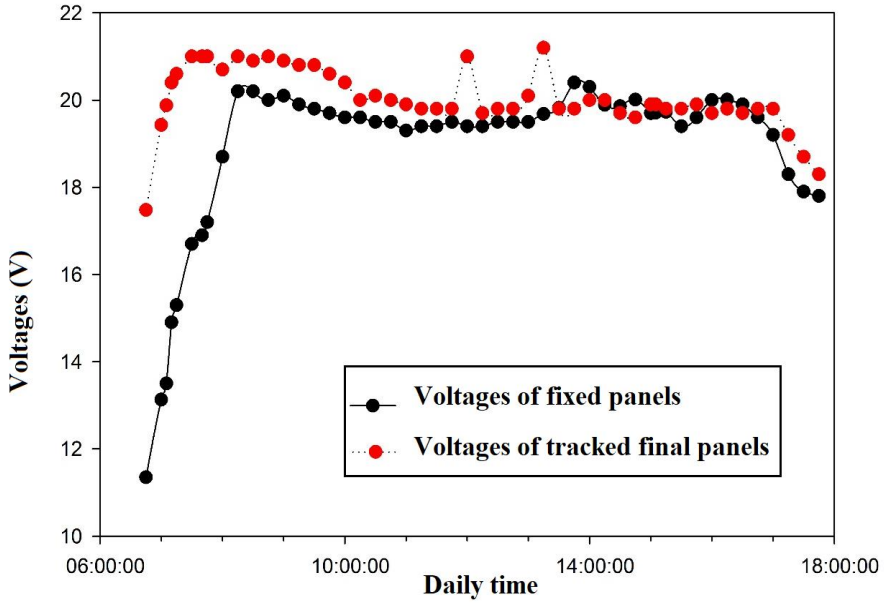

Fig. 30 Comparison of output voltages of fixed and tracked final panels during daytime hours

7-2- Voltage results

Figure 30 compares voltage profiles of the fixed and the final tracked panels. Both systems maintain relatively steady voltage around midday; however, the tracked panel sustains higher voltages during morning and late afternoon hours, aligning with improved light capture. This results in more effective

battery charging and reduces voltage drop-related losses.

Minor voltage fluctuations in the fixed panel curve, corresponding to partial shading or angle mismatch, are smoothed out in the tracked system due to continual orientation adjustment. The higher usable voltage range supports enhanced power electronics efficiency downstream in the lighting system.

7-3- Current analysis

As seen in Figure 31, the tracked panel demonstrates a higher current output especially during morning and evening hours when the sun is at lower angles, where fixed panels face significant orientation losses. Around the midday peak, both systems show high current outputs, but the tracking system consistently surpasses the fixed panel by 10-15%.

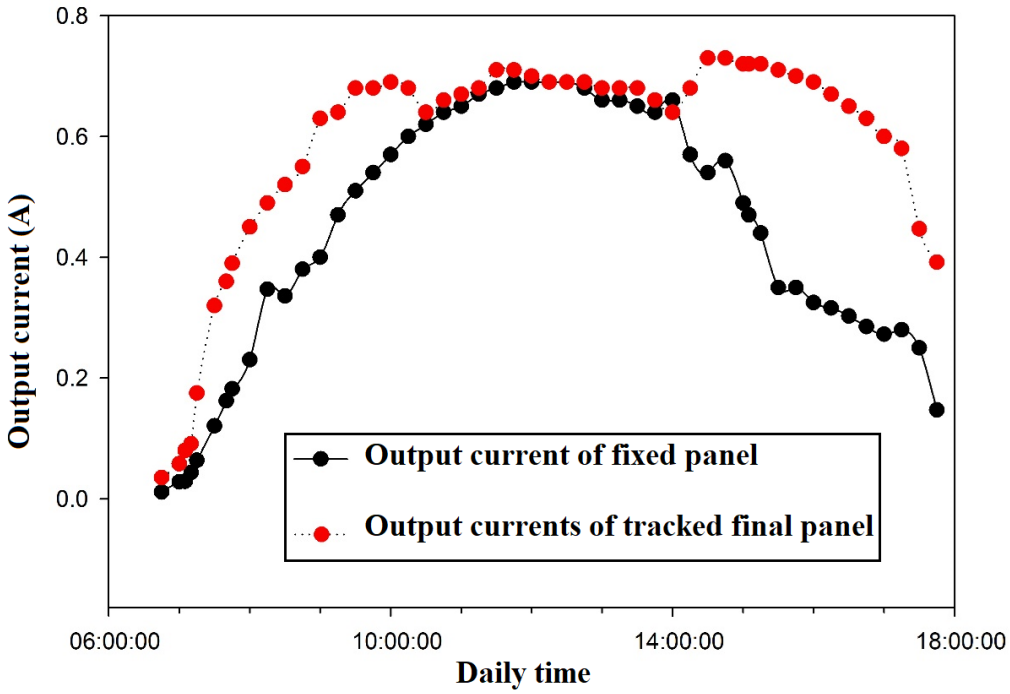

Fig. 31 Comparison of the output currents of fixed and tracked final panels during daytime hours

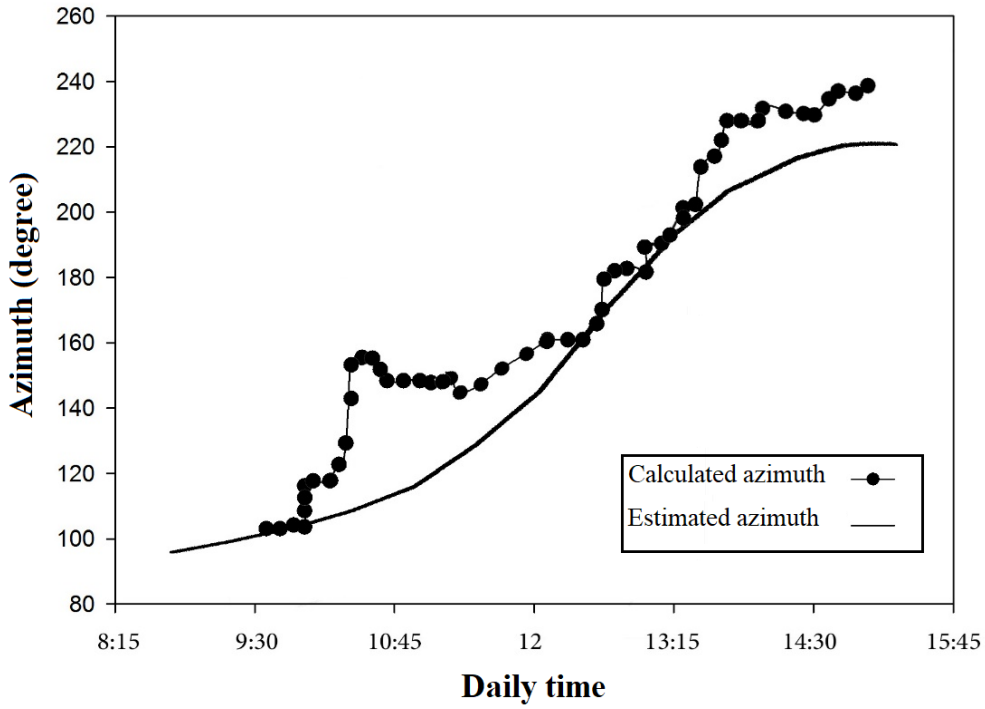

Fig. 32 The azimuth calculated practically in the first stage developed tracking and the azimuth estimated from the mentioned references.

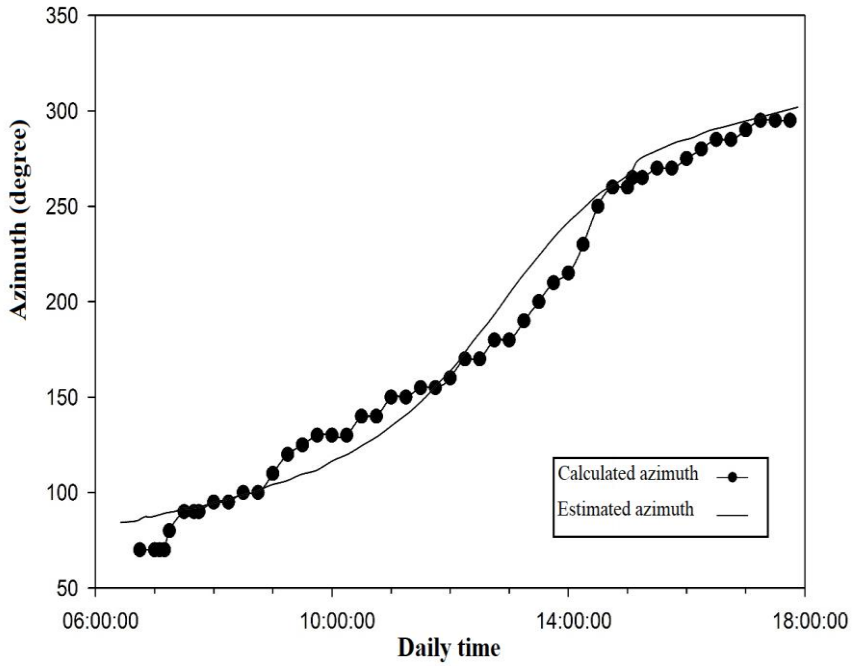

Fig. 33 The azimuth calculated practically in the final developed tracking and the azimuth estimated from the mentioned references.

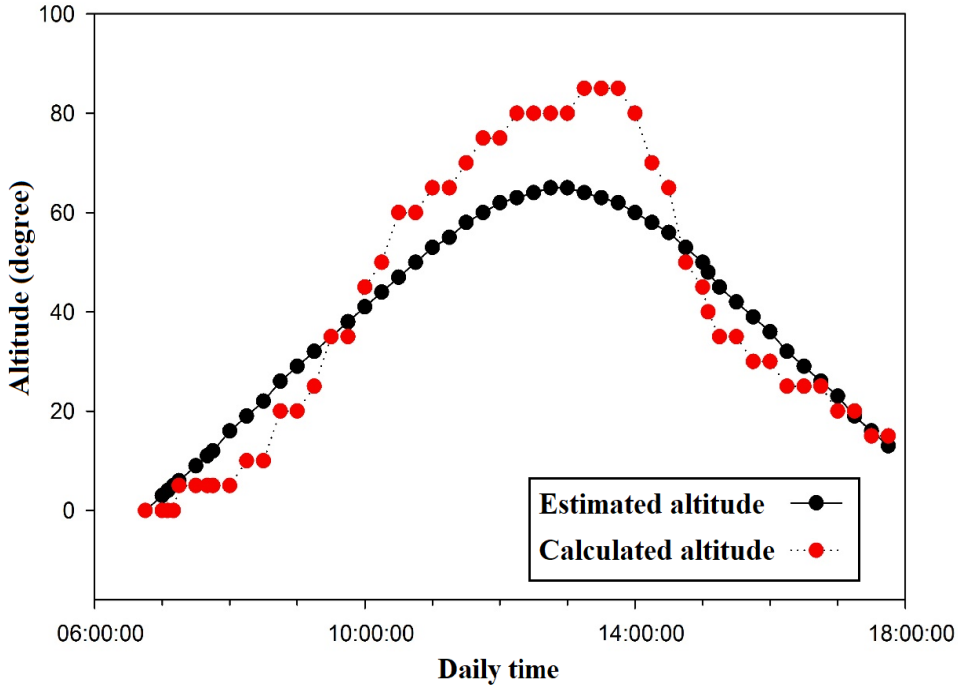

Fig. 34 Altitude calculated practically in the final developed tracking and altitude estimated from the mentioned references

7-4- Solar coordinate tracking performance

Figure 32 compares the measured azimuth angle from the final tracking system with reference values obtained from Australian geographic datasets. The tracking system closely follows the sun's path with minimal error, maintaining stable operation throughout most daylight hours.

Small deviations observed in early morning hours indicate initial sensor startup delays or minor mechanical lag in actuator response. By

mid-morning, tracking stabilizes to within ±2 degrees of the reference and remains so until late afternoon.

Figure 33 compares estimated and actual azimuth tracking angles confirming strong correlation and reliable sensor feedback integration. This validates both the electro-optical sensor design and the control circuit's processing accuracy.

Figure 34 presents the altitude angle tracking performance. Despite the intrinsic measurement challenges due to atmospheric scattering and installation constraints, the system reproduces the typical solar elevation curve reliably, aligning well with the theoretical solar altitude expected for the test site's latitude.

8- Conclusion

In this study, a dual solar–electric indoor lighting reinforcement system was designed, implemented, and experimentally evaluated. The proposed system integrates an electro-optical solar tracking mechanism with a photovoltaic subsystem and an optical daylight transmission unit, aiming to reduce electrical energy consumption for building illumination while maintaining visual comfort. The structural design, sensor configuration, and control circuits were developed with particular emphasis on simplicity, robustness, and compatibility with locally available components.

Three generations of solar tracking control circuits were systematically investigated and refined. Experimental results demonstrate that the progressive elimination of analog instabilities and noise through diode–relay logic and buffer-based signal conditioning significantly improved tracking stability and accuracy. The final developed tracking system maintained close alignment with the sun's azimuth and altitude throughout daylight hours, resulting in a substantial enhancement of photovoltaic power output compared to a fixed-panel configuration. The tracked system achieved approximately 60% higher daily energy harvest, alongside improved voltage and current stability, which are critical for reliable battery charging and lighting operation.

In addition to electrical power generation, the optical subsystem effectively transmitted natural daylight indoors, complementing the photovoltaic contribution and further reducing reliance on artificial lighting during daytime. The integration of illumination control based on standard lux requirements ensured visual comfort across different indoor environments. Collectively, these results confirm the feasibility and effectiveness of the proposed dual-mode lighting system as a practical approach for energy-efficient building illumination.

The present study was subject to certain limitations. Long-term durability under extended environmental exposure, mechanical wear of moving components, and large-scale economic assessment were not comprehensively investigated. Furthermore, sensor geometry optimization and adaptive control under extreme weather variability were beyond the scope of the current experimental campaign. Addressing these aspects would provide a more complete assessment of system performance and long-term viability.

Recommendations for future works

- Further exploration of sensor structural optimization to maximize photovoltaic output performance.
- Comprehensive investigation of environmental factors affecting the dual-mode solar-electric lighting system's operational stability and efficiency.

This research provides a solid foundation for advancing practical solar tracking solutions tailored to regional climatic conditions, encouraging further innovation and adoption of hybrid energy-efficient lighting technologies.

References

[1] Alshaabani, A. (2024). Developing the design of single-axis sun sensor solar tracking system. *Energies*, *17*(14), 3442.

[2] Pawar, P., Yadav, A., Makwana, P., & Patil, S. (2018). Solar tracking system using Arduino. *International Journal of Scientific & Engineering Research*, *9*(2), 102-104.

[3] Baouche, F. Z., Abderezzak, B., Ladmi, A., Arbaoui, K., Suciu, G., Mihaltan, T. C., ... & Țurcanu, F. E. (2022). Design and simulation of a solar tracking system for PV. *Applied Sciences*, *12*(19), 9682.

[4] Kaur, T., Mahajan, S., Verma, S., & Gambhir, J. (2016, July). Arduino based low cost active dual axis solar tracker. In *2016 IEEE 1st International Conference on Power Electronics, Intelligent Control and Energy Systems (ICPEICES)* (pp. 1-5). IEEE.

[5] Jamroen, C., Fongkerd, C., Krongpha, W., Komkum, P., Pirayawaraporn, A., & Chindakham, N. (2021). A novel UV sensor-based dual-axis solar tracking system: Implementation and performance analysis. *Applied Energy*, *299*, 117295.

[6] Badr, F., Radwan, A., Ahmed, M., & Hamed, A. M. (2022). Performance assessment of a dual-axis solar tracker for concentrator photovoltaic systems. *International Journal of Energy Research*, *46*(10), 13424-13440.

[7] Al-Othman, A., Younes, T., Al-Adwan, I., Al Khawaldah, M., Alauthman, H., Alkhedher, M., & Ramadan, M. (2023). An experimental study on hybrid control of a solar tracking system to maximize energy harvesting in Jordan. *Solar Energy*, *263*, 111931.

[8] Larico, E. R. A., & Gutierrez, A. C. (2022). Solar tracking system with photovoltaic cells: Experimental analysis at high altitudes. *International Journal of Renewable Energy Development*, *11*(3), 630.

[9] Chaithralakshmi, V. G., & Anamika, P. (2024, April). Design and implementation of sun tracking solar power system. In *Women in Optics and Photonics in India 2023* (Vol. 13108, p. 131080W). SPIE.

[10] Mamodiya, U., & Tiwari, N. (2023). Dual-axis solar tracking system with different control strategies for improved energy efficiency. *Computers and Electrical Engineering*, *111*, 108920.

[11] Wu, C. H., Wang, H. C., & Chang, H. Y. (2022). Dual-axis solar tracker with satellite compass and inclinometer for automatic positioning and tracking. *Energy for Sustainable Development*, *66*, 308-318.

[12] Kazem, H. A., Chaichan, M. T., Al-Waeli, A. H., & Sopian, K. (2024). Dual axis solar photovoltaic trackers: An in-depth review. *Energy Sources, Part A: Recovery, Utilization, and Environmental Effects*, *46*(1), 15331-15356.

[13] Rodriguez-Leon, A. I., Ordóñez, C., & Santamaria, R. (2025). Simulating the Helicase Enzymatic Action on ds-DNA: A First-Principles Molecular Dynamics Study. *ACS omega*, *10*(4), 3627-3639.

[14] Rodríguez-Gallegos, C. D., Gandhi, O., Panda, S. K., & Reindl, T. (2020). On the PV tracker performance: tracking the sun versus tracking the best orientation. *IEEE Journal of Photovoltaics*, *10*(5), 1474-1480.

[15] Al-Saadi, Y. R., Tapou, M. S., Badi, A. A., Abdulla, S., & Diykh, M. (2022). Developing smart self orienting solar tracker for mobile PV power generation systems. *IEEe Access*, *10*, 79090-79099.

[16] Mathimurugan, V. R., Karthick, V., Gokulnath, R., & Subramaniam, G. (2024, March). Smart Self Orienting Solar Tracker for PV Power Generation System. In *2024 2nd International Conference on Artificial Intelligence and Machine Learning Applications Theme: Healthcare and Internet of Things (AIMLA)* (pp. 1-5). IEEE.

[17] Lastya, H. A., Away, Y., Sara, I. D., & Novandri, A. (2025). ANFIS Parallelization Control on Triple-Axis

Sun Tracker to Minimize Solar Rays Incidence Angle on Photovoltaic. *IEEE Access*.

[18] Wang, Y., Fei, Y., Yang, T., Luo, Z., Xu, Y., Su, B., & Lin, X. (2023). Nanotechnology for ultrafast nucleic acid amplification. *Nano Today*, *48*, 101749.

[19] Eldin, S. S., Abd-Elhady, M. S., & Kandil, H. A. (2016). Feasibility of solar tracking systems for PV panels in hot and cold regions. *Renewable Energy*, *85*, 228-233.